analytical chemistry

pubs.acs.org/ac Article

StaphAIR: A Label-Free Antigen Microarray Approach to Detecting Anti-*Staphylococcus aureus* Antibody Responses in Orthopedic Infections

Alanna M. Klose, John L. Daiss, Lananh Ho, Christopher A. Beck, Christopher C. Striemer, Gowrishankar Muthukrishnan,*,# and Benjamin L. Miller*,#

Cite This: *Anal. Chem.* 2021, 93, 13580−13588 Read Online

ACCESS | Metrics & More | Article Recommendations | Supporting Information

ABSTRACT: Arrayed imaging reflectometry (AIR) is an optical biosensor platform for simple, multiplex measurement of antigen-specific antibody responses in patient blood samples. Here, we report the development of StaphAIR, an 8-plex *Staphylococcus aureus* antigen array on the AIR platform for profiling antigen-specific anti-*S. aureus* humoral immune responses. Initial validation experiments with mouse and humanized monoclonal antibodies against the *S. aureus* autolysin glucosaminidase (Gmd) domain, and subsequent testing with dilution series of pooled positive human serum confirmed analytically robust behavior of the array, with all antigens displaying Langmuir-type dose−response curves. Testing a cohort of 82 patients with *S. aureus* musculoskeletal infections (MSKI) and 30 healthy individuals enabled discrimination of individual patient responses to different *S. aureus* antigens, with statistical significance between osteomyelitis patients and controls obtained overall for four individual antigens (IsdA, IsdB, Gmd, and SCIN). Multivariate analyses of the antibody titers obtained from StaphAIR revealed its utility as a potential diagnostic tool for detecting *S. aureus* MSKI (area under the receiver operating characteristic curve (AUC) > 0.85). We conclude that StaphAIR has utility as a high-throughput immunoassay for studying and diagnosing osteomyelitis in patients.

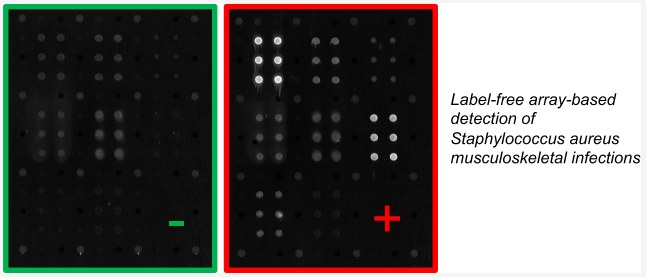

Staphylococcus aureus has been and remains the primary pathogen in infection of surgical sites and orthopedic implants.[1−3] Diagnosis of orthopedic infections can be challenging due to the complexity of sampling deep tissue sites, the requirement for repeated testing, the need to measure multiple and nonspecific biomarkers, and the frequent use of complicated imaging techniques.[3,4] To address these issues, we have been developing simple immunoassay techniques to identify ongoing *S. aureus* infections. The primary elements thus far have been multianalyte immunoassays (Luminex) that measure blood-borne antibodies against highly conserved, widely expressed *S. aureus* proteins.[5−7] These immunoassays have been successful for primary diagnosis of patients experiencing orthopedic infections (AUC > 0.85) that can otherwise take days or weeks to identify using standard clinical diagnostic protocols.[5−7]

While our work with the Luminex system demonstrated the utility of a multiplex antigen test for detecting *S. aureus* orthopedic infections, the workflow of the assay format was challenging. Additionally, interest in expanding the multiplex assay to a broader set of antigens led us to examine platforms that would simplify this process. What is needed is a robust diagnostic platform on which serum-based, multianalyte immunoassays can be run reproducibly and inexpensively while providing timely results. To that end, we report preliminary development and testing of an *S. aureus* antigen array on the arrayed imaging reflectometry (AIR) sensor platform.[8] AIR's key attributes include the following: (1) an ability to quantify 100 or more targets in a single sample; (2) speed: it can achieve adequate precision in as little as 1 h; (3) sample-sparing: it consumes only microliters of serum samples; (4) no secondary label required; and (5) broad dynamic range (3−5 orders of magnitude).

EXPERIMENTAL SECTION

Patient Samples. All patient samples were collected under protocols approved by the University of Rochester's Research Subjects Review Board (RSRB) as part of our previous Luminex assay development program. These protocols explicitly allowed the collection, storage, and use of samples for future developments such as this. Whole blood was collected into red-topped serum collection tubes. The blood was allowed to clot (0.5−12

Received: June 24, 2021
Accepted: September 20, 2021
Published: October 1, 2021

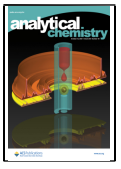

https://doi.org/10.1021/acs.analchem.1c02658
Anal. Chem. 2021, 93, 13580−13588

Table 1. Solutions Used for the Production of StaphAIR Microarrays

probe no.	antibody/ antigen	final concentration (μg/mL)	antibody/antigen volume (μL)	volume mPBS pH 5.8 (μL)	volume pH 7.4 PBS (μL)	volume of 9 μM avidin	volume of 9 μM streptavidin	volume 25% trehalose (μL)
1	anti-FITC 3	100	0.8	8.4				0.8
2	anti-FITC 2	250	1.9	7.3				0.8
3	anti-FITC 1	500	3.8	5.4				0.8
4	IsdB	500	1.7	7.5				0.8
5	IsdH	250	3.2	6.0				0.8
6	Gmd	600	4.0	5.2				0.8
7	SCIN	1950	3.0		2.2	4.0		0.8
8	Hla	500	2.2	7.0				0.8
9	IsdA	500	0.9	3.7			4.6	0.8
10	Amd	300	2.5	6.7				0.8
11	CHIPS	500	1.9	7.3				0.8

h, room temperature (RT)) and then processed by centrifugation to yield serum. Aliquots of serum were then labeled and stored in screw-capped tubes at − 80 °C until use.

***S. aureus* Antigens.** Recombinant *S. aureus* antigens were selected and produced with a biotin tag as described previously.[5−7,9,10] Briefly, these full-length proteins represent different functional classes including the following: (i) iron acquisition proteins, specifically, the iron-regulated surface determinant proteins (IsdA, IsdB, and IsdH); (ii) cell division proteins, in this case, the autolysin domains glucosaminidase (Gmd) and amidase (Amd); and (iii) immune evasion proteins and secreted toxins, chemotaxis inhibitory protein of *Staphylococcus* (CHIPS), staphylococcal complement inhibitory protein (SCIN), and α-hemolysin (Hla).

Immunochemicals and Immunoassay Reagents. Anti-fluorescein (FITC) (goat polyclonal) and bovine serum albumin (BSA) were purchased from Rockland Immunochemicals. Fetal bovine serum (FBS) was purchased from Gibco. Affinipure goat anti-human and goat anti-mouse IgG Fc-gamma fragment-specific polyclonal antibodies were purchased from Jackson ImmunoResearch Laboratories, Inc. Murine IgG1 monoclonal antibody anti-Gmd 1C11 and a humanized variant have been described previously.[11−13]

Antigen Microarray Preparation. Silicon/silicon dioxide AIR substrates with a base oxide thickness of 1384 Å and coated with an amine-reactive surface (hereafter described as "chips") were purchased from Adarza BioSystems, Inc. The protein probe mixtures comprising the microarray were pipetted into individual wells of a 384-well plate in 10 μL volumes each (formulations shown in Table 1). Prior to probe preparation, the recombinant *S. aureus* antigens (IsdA, IsdB, IsdH, Gmd, Hla, Amd, and CHIPS) were dialyzed (50 μL volume, dialyzed using 20 kDa molecular weight cutoff slide-a-lyzer dialysis cups floating in a beaker of buffer stirred slowly with a magnetic stir bar) for 1.5 h at RT in modified PBS (mPBS: 150 mM NaCl, 10 mM Na_2HPO_4, and 10 mM NaH_2PO_4, pH 5.8) to remove components from the stock solutions including glycerol and Tris−HCl that interfere with protein attachment to the chip surface.[14] Following dialysis, the *S. aureus* antigens IsdB, IsdH, Gmd, Hla, Amd, and CHIPS were diluted in mPBS. Early direct deposition experiments with ISDA and SCIN were unsuccessful, so AviTag-biotinylated and -dialyzed IsdA was incubated with streptavidin protein in mPBS for 1 h at RT. Undialyzed *S. aureus* antigen SCIN was incubated with avidin protein in PBS (137 mM NaCl, 2.7 mM KCl, 10 mM Na_2HPO_4, 1.76 mM KH_2PO_4·H_2O, pH 7.4) for 1 h at RT. The use of streptavidin and avidin improved baseline deposition thickness and preserved antigenicity of the IsdA and SCIN antigens, respectively.[15] This treatment was not necessary for the other probes on the array because each probe operates independently of the others. Three different concentrations of the intra-chip correction probe (anti-fluorescein isothiocyanate, anti-FITC) were formulated from anti-FITC antibody (dialyzed for 4 h at 4 °C in mPBS to remove sodium azide) and mPBS. All probe solutions contained trehalose as an additive to improve spot morphology.[16] Optimized print solutions used for the production of all arrays are shown in Table 1. An SX sciFLEXARRAYER (Scienion A.G.; Berlin, Germany) with a PDC70 capillary with type 4 coating was used to print a microarray of probe spots (Figure 2a) onto chips mounted onto adhesive strips inside a controlled humidity chamber at 72% ± 4% RH. Droplets were between 300 and 350 pL in volume, as measured by the instrument. The chips remained in the humidified chamber for 30 min to ensure covalent attachment of the protein antigens to the surface.

Antigen Microarray Blocking and Stabilization. The microarrayed chips were removed from the humidified microspotting chamber and immediately placed into wells of a 96-well plate, each containing 300 μL of 50 mM NaOAc, pH 5.0, for 5 min to prevent smearing of any unadsorbed probes onto nearby areas of the amine-reactive chip surface. The chips were then incubated in 1% BSA in NaOAc, pH 5.0, for 30 min to block the background from nonspecific adsorption and then transferred to wells containing a second blocking solution of 20% FBS in assay wash buffer (AWB: mPBS with 0.005% Tween-20, pH 7.2) for 30 min. Following blocking, chips were transferred to wells containing AWB and incubated for 10 min before being transferred to wells containing StabilCoat Plus and incubating for 30 min. All incubation steps were performed at RT with orbital shaking (300 rpm). The stabilized chips were placed into a 40 °C oven for 1 h before being stored in a sealed Mylar bag with a desiccant and nitrogen gas at 4 °C until use in immunoassay experiments.

Measurement of Antibody Binding. All incubations were performed with stabilized microarrayed chips mounted on adhesive combs inserted into individual wells of a 96-well plate on an orbital shaker at 300 rpm. The assay diluent in all cases was Adarza Assay Buffer (Adarza BioSystems, Inc., St. Louis, MO) with 20% filtered FBS. After either the overnight (ON) 4 °C, 1 h RT, or 1 h 37 °C primary incubation, all chips were transferred to AWB for 5−10 min and exposed to a 1 h RT amplification step that consisted of incubation with an anti-IgG specific for the primary IgG. Chips underwent a final incubation in AWB for 10 min before being rinsed in Nanopure water and dried under a stream of nitrogen gas. Control chips underwent exactly the

https://doi.org/10.1021/acs.analchem.1c02658
Anal. Chem. 2021, 93, 13580−13588

same process but were only exposed to the assay diluent during the primary incubation step.

Primary incubation conditions and antibody/serum concentrations for all samples were as follows:

- mouse anti-Gmd 1 C11 antibody:
  (1) 1 h RT incubation (25, 20, 15, 10, 5, 2.5, 1, 0.1, and 0.01 μg/mL)
  (2) 1 h 37 °C incubation (25, 10, 5, 1, 0.5, 0.1, 0.01, and 0.001 μg/mL)
  (3) ON 4 °C incubation (25, 10, 5, 1, 0.5, 0.1, 0.01, 0.001, and 0.0001 μg/mL)
- humanized anti-Gmd 1C11 antibody:
  (1) 1 h RT incubation and overnight 4 °C incubation (1, 0.25, 0.1, 1×10^{-2},1×10^{-3},1×10^{-4},1×10^{-5}, and 1×10^{-6} μg/mL)
- pooled positive human serum dilutions:
  (1) 1 h RT incubation (1:50, 1:100, 1:250, 1:500, 1:1000, 1:5000, and 1:10,000)
  (2) ON 4 °C incubation (1:50, 1:100, 1:250, 1:500, 1:1000, 1:5000, 1:10,000, 1:50,000, and 1:100,000)
- single-donor human serum samples:
  (1) 1 h RT incubation at 1:1000 dilution

Imaging with Arrayed Imaging Reflectometry and Data Analysis. AIR detects molecular binding by measuring the perturbation of a near-zero reflectance condition of light of fixed wavelength (632.8 nm), polarization (s-polarized), and angle of incidence (70.7°), interacting with a set of capture molecules microarrayed on a Si/SiO_2 planar surface coated with an adhesion chemistry capable of covalently binding the capture molecules during the microarraying process. The near-zero reflectance is established by tuning the thickness of the oxide, amine-reactive chemistry, and probe molecules. The binding of analyte molecules to immobilized probes increases the thickness of the surface and is detected as an increase in reflectance. Reflectance and thickness are not linearly related, so it is important to convert reflectance to thickness (a more accurate portrayal of the amount of material deposited and bound) for comparison between biological samples.[17] The reflectance is captured by a charge-coupled device (CCD) and measured as pixel intensity, from which the thickness of the surface is inferred from a parabolic model generated by cross-calibration to spectroscopic ellipsometry (Figure 1). The dynamic range of the instrument is expanded by acquiring sequential images of the same array at multiple CCD exposure times in milliseconds (ms). This is a quick process, requiring less than 1 min to acquire 5−6 images per array using automated software. As seen in Figure 1, higher-exposure images improve AIR sensitivity for probe spots that are thin and closer to the antireflective condition (Figure 1, arrow a), while lower-exposure images improve sensitivity for probe spots that are thick and farther from the antireflective condition (Figure 1, arrow b). Therefore, if a probe binds a large amount of analyte and becomes overexposed at a higher exposure, a lower-exposure image is used for quantification. Likewise, if a probe binds a small amount of analyte, then a higher-exposure image is used to detect changes in reflectance resulting from that increase in mass. Additionally, the use of multiple CCD exposure times means that the baseline probe thicknesses do not need to be identical to achieve high assay sensitivity: each probe type is compared to its own baseline thickness and is treated independently of other probes in the multiplex array.

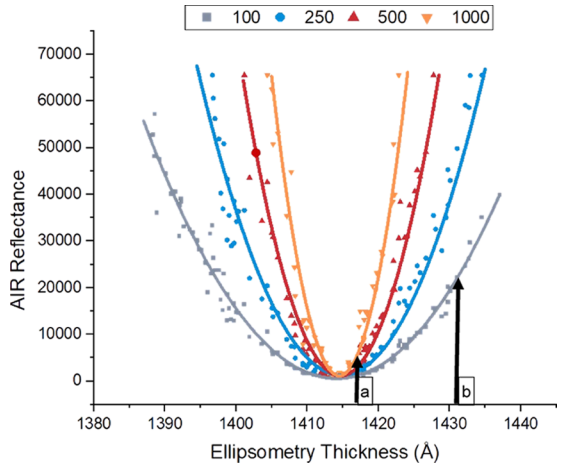

Figure 1. AIR enables precise determination of thickness changes as ligands bind to an immobilized substrate. Si/SiO_2 chips with increase oxide thickness. Each chip's AIR reflectance from images at 100, 250, 500, and 1000 ms CCD exposure times was cross-calibrated with spectroscopic ellipsometry, and a parabolic fit was applied to data from each exposure. Higher exposure-images increase sensitivity close to the antireflective condition (arrow a), while lower exposure-images increase sensitivity farther from the antireflective condition (arrow b).

Each microarray chip was imaged by a prototype AIR imaging system (Adarza BioSystems; St. Louis, MO) containing a temperature-controlled CCD with custom software to acquire images at 10, 50,100, 250, 500, and 1000 ms exposures with dark frame subtraction. A representative chip imaged at 50, 100, 250, and 500 ms exposures is presented in Figure 2b. Median probe intensities were analyzed from AIR images and converted to median thickness using the Adarza Biosystems ZIVA data analysis tool at appropriate exposures, avoiding saturation and blooming in the CCD images. Probe spots with major defects or debris were manually flagged and eliminated, and minor defects in spot quality were automatically identified by the software and excluded from the measurement. While we remove probe spots with major defects manually, this process has been automated in software by Adarza Biosystems for the commercial version of AIR. The average corrected *S. aureus* antigen probe thickness ($\overline{T}$) was calculated by averaging the median thicknesses of replicate probe spots, each of which was corrected by subtracting the average median thickness of the surrounding anti-FITC correction probes (Figure 2c). The anti-FITC spots serve as controls for nonspecific binding, and are also used as an intra-chip correction to account for local differences in chip thickness. Bright *S. aureus* antigen probes were corrected by FITC1, medium probes corrected with FITC2, and dim probes corrected by FITC3. Once defined, the choice of correction FITC was held constant for all analyte and control chips. (FITC1: SCIN and Hla; FITC2: IsdB, IsdH, and CHIPS; FITC3: Gmd, IsdA, and Amd). Average corrected thickness for each antigen was calculated from four to six replicate *S. aureus* antigen probes on each chip (variation is due to debris and flagged spots) and four surrounding anti-FITC correction probes for each *S. aureus* antigen probe. The error was calculated as the standard deviation (SD) of the average corrected *S. aureus* antigen probe thickness. $\overline{T}_{change}$, a measure of antibody binding to antigen probe was calculated by subtracting $\overline{T}_{control}$ (measured from the chip exposed to the assay diluent only) from $\overline{T}_{sample}$ (measured from a chip exposed to a sample). The overall approach to data analysis is highlighted in Figure 2c. While we

https://doi.org/10.1021/acs.analchem.1c02658
Anal. Chem. 2021, 93, 13580−13588

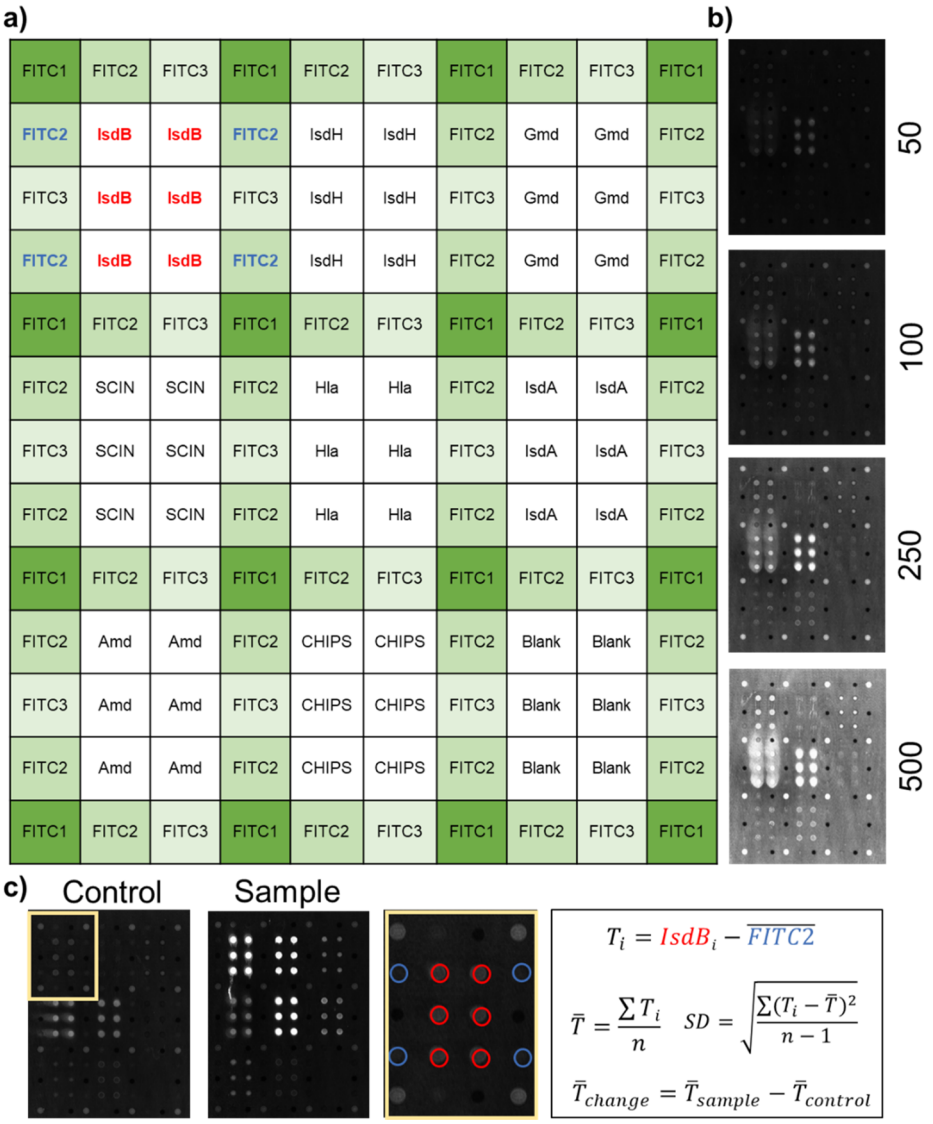

Figure 2. AIR microarray probe layout and analysis. (a) Each box indicates a single probe spot on the microarray. (b) Four different CCD exposure times (ms) of the same control chip are provided to demonstrate how probes of different baseline intensity are able to be measured accurately by AIR. (c) Intra-chip correction and calculation of average probe thickness, standard deviation, and average change of probe thickness using the response to IsdB as an example. *IsdB* is the median thickness of a single probe, n is the number of IsdB probes ($n = 6$ if no debris requires a probe spot to be removed from analysis), $\overline{FITC2}$ is the average median thickness of four anti-FITC2 control probes, T_i is an individual corrected IsdB probe thickness, $\bar{T}$ is the average corrected IsdB test probe thickness, *SD* is the standard deviation of corrected probe spots, and T_{change} is the thickness change measured when an antibody target binds to antigen probe spots. The same calculations were performed for the other seven *S. aureus* antigen probes, with attention to probe brightness, where bright probes were corrected by FITC1, medium probes corrected with FITC2, and dim probes corrected by FITC3.

have not found the need for an on-chip positive control in our work to date, we have confirmed previously that anti-human IgG antibody spots could potentially be used for this purpose (Miller et al., unpublished results).

Standard Curves. To generate standard curves for the monoclonal antibody and pooled positive serum dilutions, the control values and all experimental conditions were plotted in OriginPro 2016 (OriginLab Corporation), and a four-parameter logistic (4PL) regression (eq 1) was applied, where A_1 is the minimum thickness on the curve, A_2 is the maximum thickness on the curve, x_0 is the inflection point, and p is the slope of the curve at the inflection point

$$y = A_2 + \frac{A_1 - A_2}{1 + \left(\frac{x}{x_0}\right)^p} \quad (1)$$

The limit of the blank (LOB) was calculated from the control values for each antigen (eq 2), where μ is the mean and σ is the standard deviation. The limit of detection (LOD) was calculated from a combination of all low-concentration thickness values and standard deviations (near and below the inflection point of the logistic curve) (eq 3).[18−20]

$$\text{LOB} = \mu_{\text{blank}} + 1.645(\sigma_{\text{blank}}) \quad (2)$$

$$\text{LOD} = \text{LOB} + 1.645(\sigma_{\text{low concentration samples}}) \quad (3)$$

The single donor sera antibody binding data were generated by subtracting the thickness of the probes in the control chips ($\bar{T}_{\text{control}}$) from the thickness of corresponding probes in the chips exposed to serum ($\bar{T}_{\text{sample}}$). This was done batch by batch, where a "batch" is defined as a group of chips that was printed, blocked, and stabilized at the same time, to eliminate any variations in

https://doi.org/10.1021/acs.analchem.1c02658
Anal. Chem. 2021, 93, 13580−13588

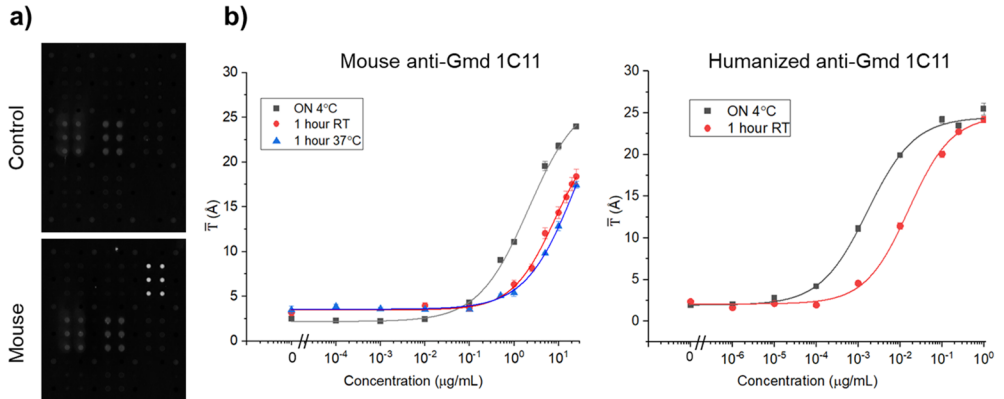

$$y = A_2 + \frac{A_1 - A_2}{1 + \left(\frac{x}{x_0}\right)^p}$$

	1 hour RT mouse anti-Gmd	1 hour 37°C mouse anti-Gmd	ON 4°C mouse anti-Gmd	1 hour RT humanized anti-Gmd	ON 4°C humanized anti-Gmd
A_1	3.5	3.6	2.2	2.1	1.9
A_2	23.8	31.4	27.5	24.7	24.5
X_0 (μg/mL)	8.3	25.2	2.1	0.016	0.0017
p	0.9	0.8	0.8	0.8	0.8
Adj. R-Square	0.9919	0.9971	0.9973	0.9918	0.9987
LOB (ng/mL)	39	190	26	0.14	0.0062
LOD (ng/mL)	130	340	40	0.29	0.023

Figure 3. Quantitative StaphAIR. The monoclonal anti-Gmd antibodies bind immobilized Gmd antigens without cross-reactivity with other *S. aureus* antigens on the array. (a) Images acquired at 50 ms CCD exposure following incubation with (Mouse) 10 μg/mL mouse anti-Gmd 1C11 and (Humanized) 10 ng/mL anti-Gmd 1C11. (b) Binding behavior varies with incubation conditions. Overnight incubation at 4 °C improves LODs for mouse and humanized monoclonal anti-Gmd 1C11.

microarray preparation and to ensure parity between batches. Average measurements for positive and negative serum samples were calculated by averaging the values for each antigen across all grouped samples. Error bars in these cases represent standard error.

Data Visualization and Statistical Analyses. The StaphAIR antibody response heat map was generated using Pandas[21] and Seaborn[22] to visualize max/min normalized $\overline{T}_{change}$ for all single-donor serum samples. Max/min normalization was performed using the maximum and minimum thickness change data for each antigen, resulting in normalized values between 0 and 1. Comparisons of eight-array antibody measurements across "control" and "infected patients" were performed using one-way ANOVA. StaphAIR antibody measurements were assessed for their predictive ability to discriminate infected patients from control subjects using receiver operating characteristic (ROC) curve analysis, with overall predictive accuracy summarized by the area under the ROC curve (AUC).[5−7] ROC analyses were performed for the eight StaphAIR antigens individually and in combinations. Antigen combinations were determined using the best subset selection with multivariate logistic regression models to identify groups of antibodies that best diagnosed *S. aureus* infection. Ninety-five percent confidence intervals and nonparametric estimates for the AUC were computed for each predictor. Analyses were conducted using GraphPad Prism version 9.1, SAS version 9.4, and Python v3.8.5. A p-value of <0.05 was considered significant.

RESULTS AND DISCUSSION

Relationship of Thickness Measurements and Antibody Concentrations. To validate StaphAIR as an analytical technique in which thickness measurements can be related to the target concentration, two monoclonal antibodies (mouse anti-Gmd 1C11 and humanized anti-Gmd 1C11) were serially diluted and incubated with the *S. aureus* antigen microarrays. Primary incubations were followed by the anti-IgG amplification step (i.e., addition of an unconjugated secondary goat anti-mouse or anti-human IgG) prior to analysis. Both the mouse and humanized anti-Gmd 1C11 antibodies specifically bound to the Gmd antigen immobilized on the array without cross-reactivity with other antigens on the array (Figure 3a). Then, 4PL regression fits for observed Gmd probe thicknesses after incubation with each concentration of monoclonal antibody are shown in Figure 3b. Varying the primary incubation condition between RT and 37 °C had little effect on the binding of mouse anti-Gmd to immobilized Gmd, but the ON 4 °C primary incubation did. Therefore, we incubated the humanized anti-Gmd with the array only for 1 h RT or ON 4 °C. As one might expect, implementing a longer primary incubation time enhanced the sensitivity of the assay. The ON incubation improved the LOD of both the mouse and humanized 1C11 antibodies (40 ng/mL ON, 130 ng/mL RT; 23 pg/mL ON, 290 pg/mL RT), respectively. The longer incubation time allows for more binding to occur than the 1 h incubation. Moreover, the longer incubation is likely closer to an equilibrium state than the 1 h incubation, which can affect the parameters of the 4PL regression.[23] Assuming that the secondary binding kinetics are similar, the humanized anti-Gmd 1C11 antibody seems to be a tighter binder to the Gmd probe than the mouse 1C11 antibody judging both by the 3 orders of magnitude improvement in LOD and by the location of the inflection points of the curves (X_0) 0.0017 μg/mL for the humanized antibody and 2.1 μg/mL for the mouse antibody. This could be confirmed by elimination of the optional secondary amplification step.

Serial dilutions of pooled positive human sera were used to demonstrate the functional integrity of each probe in the *S. aureus* antigen array and to determine the LOB and LOD for the 1 h RT and 4 °C ON incubation conditions for each antigen. Consistent with the monoclonal antibody titrations, it is clear from the AIR images in Figure 4a that the ON incubation bound more target antibodies at lower serum concentrations than the

https://doi.org/10.1021/acs.analchem.1c02658
Anal. Chem. 2021, 93, 13580−13588

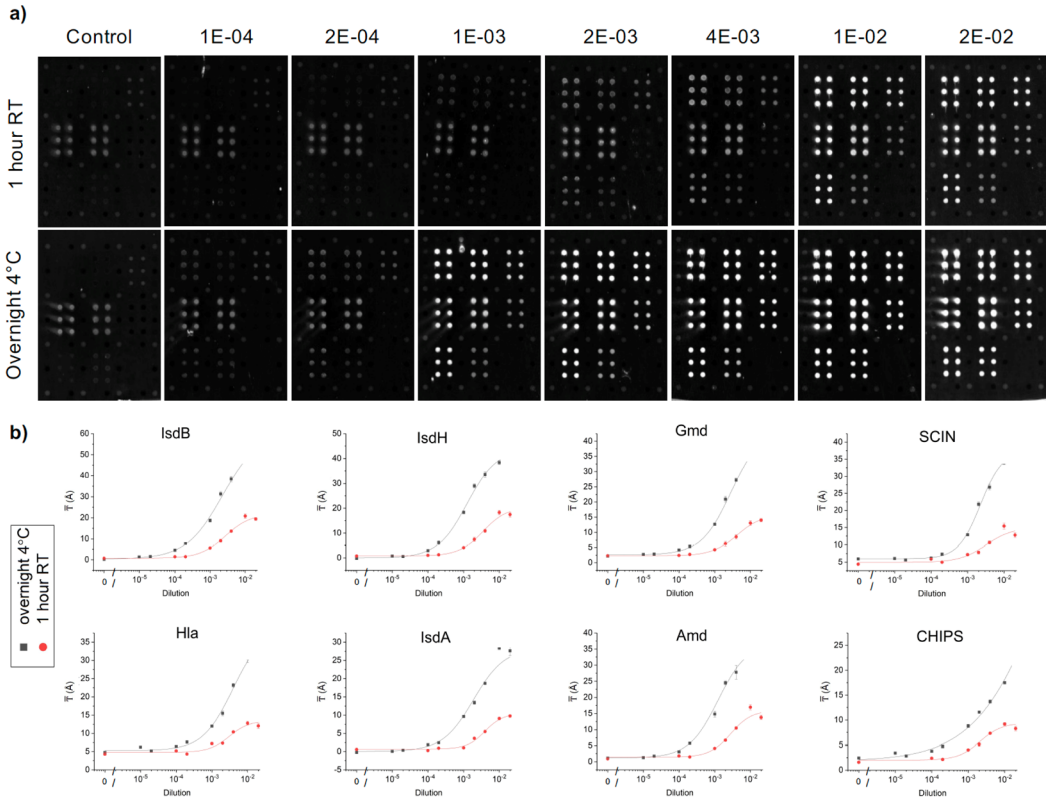

	IsdB	IsdH	Gmd	SCIN	Hla	IsdA	Amd	CHIPS
1 hour RT LOB	5.1E-05	2.0E-04	1.6E-04	2.6E-04	1.4E-04	3.0E-04	1.3E-04	1.1E-04
1 hour RT LOD	1.9E-04	4.4E-04	3.6E-04	4.7E-04	5.0E-04	5.8E-04	2.3E-04	2.3E-04
overnight 4°C LOB	3.7E-06	9.0E-06	2.2E-05	1.4E-04	2.8E-05	2.2E-06	1.4E-05	1.5E-05
overnight 4°C LOD	1.4E-05	3.1E-05	5.1E-05	2.2E-04	7.2E-05	8.0E-06	3.6E-05	3.9E-05

Figure 4. Assessment of analytic sensitivity using serial dilutions of pooled positive human sera. (a) All images were taken with a 100 ms CCD exposure time to demonstrate improved sensitivity at higher dilutions (lower antibody concentration) with 4 °C ON primary incubation. (b) Quantification of the lowest detectable concentration (most diluted sample) was performed using images at appropriate exposure times, avoiding overexposure of probes. Error bars are standard deviation of probe replicates as defined in Figure 2c. Four-parameter logistic regression analysis was performed in Origin, and fit parameters were used to calculate LODs. ON incubation extended the LOD by at least one order of magnitude for all probes except SCIN.

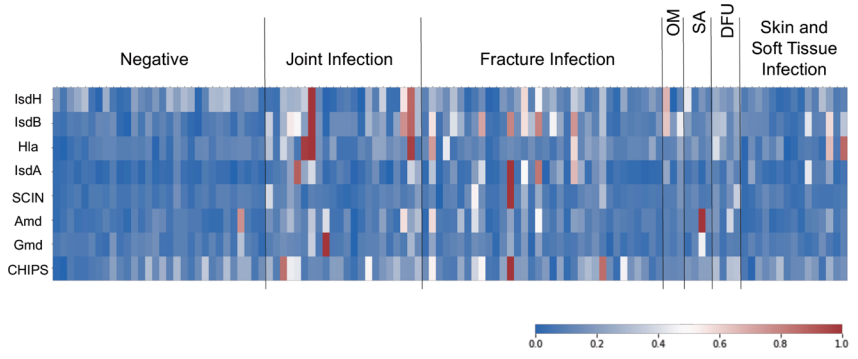

Figure 5. StaphAIR provides a quantitative analysis of the abundance of anti-*S. aureus* antibodies present in single-donor serum samples. Thickness changes were normalized to the maximum and minimum values for each antigen. OM = osteomyelitis, SA = septic arthritis, and DFU = diabetic foot ulcer.

RT incubation. Because these images were all acquired with 100 ms exposures, the probes quickly became saturated at higher concentrations. However, as discussed above, each array was imaged at multiple exposures, allowing both high- and lower-exposure images to be used for quantification, thus increasing the dynamic range of the StaphAIR platform. After plotting the thicknesses of probe spots at each dilution and fitting the data with a 4PL regression, the LOD was calculated from low-concentration samples (Figure 4b). The ON incubation not only extends the LOD by an order of magnitude for almost every probe but also nearly doubles the total amount of target bound at higher serum concentrations.

https://doi.org/10.1021/acs.analchem.1c02658
Anal. Chem. 2021, 93, 13580−13588

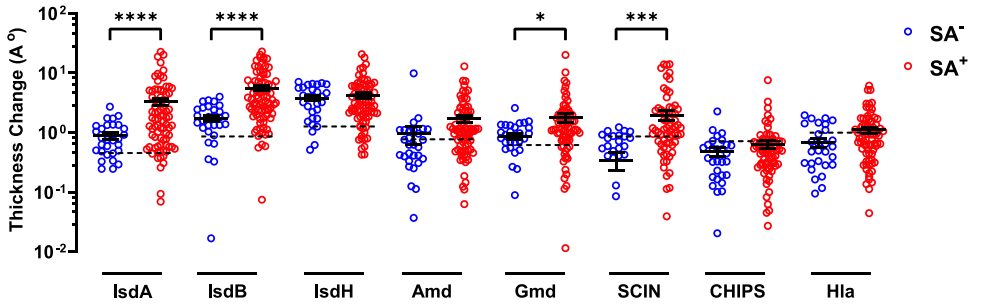

Figure 6. Levels of anti-Staphylococcal antibodies in sera from *S. aureus* MSKI patients measured in multiplex StaphAIR Immunoassays. Thickness change (reported in Ångstroms (Å)) from healthy controls ($n = 30$, SA^-) and *S. aureus*-infected patients ($n = 82$, SA^+). Data are depicted as mean +/− SD; * $p < 0.05$, ** $p < 0.01$, and *** $p < 0.001$. Dotted lines represent the minimum detectable thickness change for each antigen.

Examining the Anti-*S. aureus* Antibody Responses in Patients Using an Eight-Antigen StaphAIR Immunoassay. With an interest in developing a rapid assay for single-donor serum samples, we chose to implement a 1 h RT incubation with 1:1000 serum dilution, which is above the LOD of antibody in pooled positive sera for each antigen under that condition but low enough to demonstrate assay sensitivity. Results from 82 patients with *S. aureus* infections and 30 healthy controls are shown in Figures 5 and 6. Inspection of the heat map in Figure 5 shows a general increase in anti-*S. aureus* response for patients with active infections relative to negative (healthy) controls. Analysis of the data on an antigen-by-antigen basis shows that antibody responses to four antigens individually (IsdA, IsdB, Gmd, and SCIN) provide statistically significant discrimination between healthy and infected subjects. Some SA^- and SA^+ samples had calculated thickness changes that were below the minimum detectable thickness change (LODs in Å were calculated from the 1 h RT pooled positive exposed samples in Figure 4 minus the average of control chips). This means that those samples did not have antibody binding that was distinguishable from controls, which is expected for many SA^- samples and consistent with the high degree of variability in anti-*S. aureus* antibody responses in SA^+ samples[5] and generally in humans.[24]

Multiplex StaphAIR Immunoassay is Diagnostic of *S. aureus* MSKI. Next, we examined if thickness measurements from StaphAIR can be utilized to diagnose *S. aureus* MSKI. To formally assess this, we performed receiver operator area under the curve (AUC) characteristic analyses (Figure 7). Individual ROC curve analyses revealed that the immunodominant IsdB yielded the highest AUC of 0.778 (Figure 7A−C, **** $p < 0.0001$), with antigen Amd yielding the lowest AUC of 0.512. Importantly, we observed that the diagnostic prediction can be markedly improved by antigen combinations (Figure 7D). Multivariate ROC analyses revealed that a five-antigen combination of IsdB + Amd + IsdA + SCIN + Hla yielded a high AUC of 0.861 (**** $p < 0.0001$). Coefficients for linear combinations of antigens based on multivariate logistic regression used for development of the ROC curve analyses and comparison to standardized scoring coefficients from principal component analysis (PCA) are included in the Supporting Information.

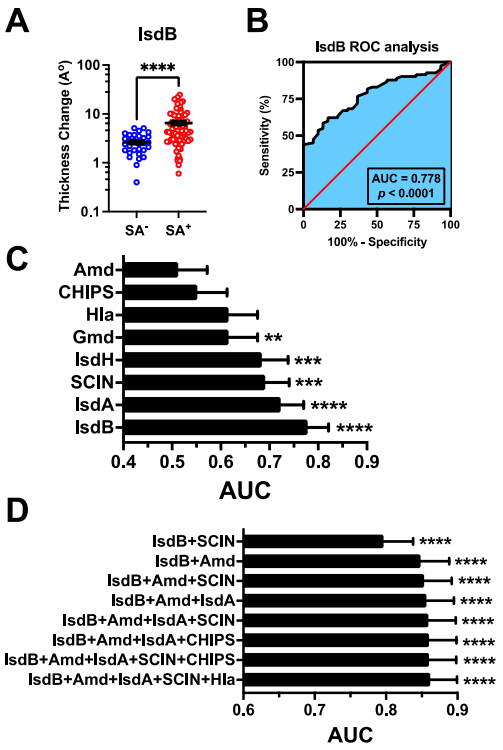

Figure 7. Diagnosis of anti-Staphylococcal antibodies in serum from *S. aureus* MSKI patients utilizing multiplex StaphAIR immunoassay. (A) IsdB-specific thickness change (reported in Ångstroms (Å)) from healthy controls ($n = 30$, SA^-) and *S. aureus* osteomyelitis patients ($n = 82$, SA^+). (B) The primary IsdB thickness change data was used to perform single antigen receiver operator curve characteristics analysis (AUC). (C) ROC curve analyses for all eight StaphAIR antigens are presented in rank order of lowest to highest AUC values. (D) Multivariate ROC analyses using two-, three-, four-, and five-antigen combinations were performed to increase diagnostic potential of StaphAIR. Note that high AUC values >0.85 were obtained in four- and five-antigen combinations. Data are depicted as mean +/− SD with significance at ** $p < 0.01$, *** $p < 0.001$, and **** $p < 0.0001$.

CONCLUSIONS

Multiplex methods for profiling the immune response of patients to *S. aureus* antigens have considerable utility in studying the basic biology of orthopedic infections and should prove useful in a diagnostic context. In particular, these methods may avoid limitations of current state-of-the-art techniques, which require direct access to the infected site and may be confounded by contamination from skin microorganisms near the access point. In a previous work, we have demonstrated the utility of AIR as a tool for profiling the immune response to infection by and immunization against viral pathogens, including influenza[17,25] and SARS-CoV-2.[26] We have also used AIR to assess autoimmunity in Sjögrens disease and systemic lupus erythematosus.[16] Here, we have provided the first demonstration of

https://doi.org/10.1021/acs.analchem.1c02658
Anal. Chem. 2021, 93, 13580−13588

the use of bacterial antigens on the AIR platform. The array is well-behaved analytically, with a quantitative dose−response behavior consistent with Langmuir surface binding. Most importantly, assessment of single-donor human samples provided good discrimination of diseased vs healthy subjects. The eight antigens had a range of diagnostic values among the several classes of orthopedic infections including prosthetic joint infections, diabetic foot ulcers, fracture-related infections, and septic arthritis.

The analytic range of StaphAIR is adequate for serum samples diluted 1:1000; it is likely that the analytic range can be greatly improved. Quantitative performance of StaphAIR can be tuned via incubation conditions, incubation time, and the inclusion or exclusion of the amplification step to achieve a variety of assay goals, including speed and high sensitivity. Overnight incubation may be useful for lower-concentration samples, and it is important to note that StaphAIR analytic sensitivity can be improved with the longer incubation times but that a shorter incubation time is sufficient for typical serum antibody samples.

As an array-based technology, AIR can be utilized for the simultaneous detection of specific antibodies for multiple antigens. In the context of antibody arrays, we have demonstrated use of up to 115-plex assays.[25] As such, expansion of the StaphAIR array to incorporate more *S. aureus* antigens should be straightforward. Use of larger arrays of antigens has enabled the discrimination of septic arthritis from PJI and DFU from skin and soft tissue infections.[7] To that end, efforts are underway to optimize the analytical performance of StaphAIR by examining the variables discussed above and extend its capabilities to a broader antigen array.

Finally, we anticipate that the multianalyte capability of StaphAIR can readily be expanded to include antigens from other common orthopedic pathogens on the same chip. While *S. aureus* is the most frequent and challenging-to-treat among orthopedic pathogens, it is not the only bacterium that causes life-changing, sometimes life-threatening, infections. In particular, we anticipate adding antigens for detection of antibodies to *S. epidermidis, Streptococcus agalactiae,* and *Cutibaceterium acnes*. With StaphAIR's capability to assess the response to as many as 115 antigens simultaneously, development of multispecies AIR chips should be both an excellent diagnostic and research tool. Pathogens that have already been examined in this way include *Clostridiodes difficile*,[27] SARS-CoV-2,[26,28] influenza virus,[29] respiratory syncytial virus,[30,31] and *Mycobacterium tuberculosis*.[32].

■ ASSOCIATED CONTENT

Supporting Information

The Supporting Information is available free of charge at https://pubs.acs.org/doi/10.1021/acs.analchem.1c02658.

Table with coefficients for linear combinations of antigens based on multivariate logistic regression models and comparison to standardized scoring coefficients from PCA (PDF)

■ AUTHOR INFORMATION

Corresponding Authors

Gowrishankar Muthukrishnan − *Department of Orthopaedics, Center for Musculoskeletal Research, University of Rochester, Rochester, New York 14627, United States*;
Email: Gowri_Shankar@urmc.rochester.edu

Benjamin L. Miller − *Department of Dermatology and Department of Biomedical Engineering, University of Rochester, Rochester, New York 14627, United States*;
orcid.org/0000-0001-9168-8047;
Email: Benjamin_Miller@urmc.rochester.edu

Authors

Alanna M. Klose − *Department of Dermatology, University of Rochester, Rochester, New York 14627, United States*

John L. Daiss − *Department of Orthopaedics, Center for Musculoskeletal Research, University of Rochester, Rochester, New York 14627, United States*

Lananh Ho − *Department of Biomedical Engineering, University of Rochester, Rochester, New York 14627, United States*

Christopher A. Beck − *Department of Orthopaedics, Center for Musculoskeletal Research and Department of Biostatistics and Computational Biology, University of Rochester, Rochester, New York 14627, United States*

Christopher C. Striemer − *Adarza BioSystems, Inc., St. Louis, Missouri 63146, United States*

Complete contact information is available at: https://pubs.acs.org/10.1021/acs.analchem.1c02658

Author Contributions

#G.M. and B.L.M. are co-senior authors.

Notes

The authors declare the following competing financial interest(s): B. L. Miller is a shareholder and consultant to Adarza BioSystems, a company commercializing the Arrayed Imaging Reflectometry (AIR) technology. C. C. Striemer is an employee of and shareholder in Adarza BioSystems.

■ ACKNOWLEDGMENTS

The authors are grateful to the patients and research volunteers that participated in this study and to Prof. Edward M. Schwarz for helpful discussions. This research was supported by a pilot award administered by the National Institute of Arthritis and Musculoskeletal and Skin Diseases, National Institutes of Health P30 AR069655 award with additional support from Center of Research Translation on the Osteoimmunology of Bone Infection (CoRTOBI), 5P0AR0720000, and AO Trauma Clinical Priority Program on Bone Infection.

■ REFERENCES

(1) Inzana, J. A.; Schwarz, E. M.; Kates, S. L.; Awad, H. A. *Biomaterials* **2016**, *81*, 58−71.

(2) Muthukrishnan, G.; Masters, E. A.; Daiss, J. L.; Schwarz, E. M. *Curr Osteoporos Rep* **2019**, *17*, 395−404.

(3) Ricciardi, B. F.; Muthukrishnan, G.; Masters, E. A.; Kaplan, N.; Daiss, J. L.; Schwarz, E. M. *J Orthop Res* **2020**, 1423.

(4) Masters, E. A.; Trombetta, R. P.; de Mesy Bentley, K. L.; Boyce, B. F.; Gill, A. L.; Gill, S. R.; Nishitani, K.; Ishikawa, M.; Morita, Y.; Ito, H.; Bello-Irizarry, S. N.; Ninomiya, M.; Brodell, J. D.; Lee, C. C.; Hao, S. P.; Oh, I.; Xie, C.; Awad, H. A.; Daiss, J. L.; Owen, J. R.; Kates, S. L.; Schwarz, E. M.; Muthukrishnan, G. *Bone Research* **2019**, *7*, 20.

(5) Nishitani, K.; Beck, C. A.; Rosenberg, A. F.; Kates, S. L.; Schwarz, E. M.; Daiss, J. L. *Clin Orthop Relat Res* **2015**, *473*, 2735−2749.

(6) Oh, I.; Muthukrishnan, G.; Ninomiya, M. J.; Brodell, J. D., Jr.; Smith, B. L.; Lee, C. C.; Gill, S. R.; Beck, C. A.; Schwarz, E. M.; Daiss, J. L. *Infect. Immun.* **2018**, *86*, No. e00629.

(7) Muthukrishnan, G.; Soin, S.; Beck, C. A.; Grier, A.; Brodell, J. D., Jr.; Lee, C. C.; Ackert-Bicknell, C. L.; Lee, F. E.; Schwarz, E. M.; Daiss, J. L. *Immunohorizons* **2020**, *4*, 339−351.

(8) Mace, C. R.; Striemer, C. C.; Miller, B. L. *Anal. Chem.* **2006**, *78*, 5578−5583.
(9) Muthukrishnan, G.; Beck, C. A.; Owen, J. R.; Xie, C.; Kates, S. L.; Daiss, J. L. *J Orthop Res* **2021**, 2169.
(10) Fu, W.; He, W.; Ren, Y.; Li, Z.; Liu, J.; Liu, Y.; Xie, Z.; Xu, J.; Bi, Q.; Kong, M.; Lee, C. C.; Daiss, J. L.; Muthukrishnan, G.; Owen, J. R.; Kates, S. L.; Peng, J.; Xie, C. *J Orthop Res* **2021**, *39*, 265−273.
(11) Varrone, J. J.; de Mesy Bentley, K. L.; Bello-Irizarry, S. N.; Nishitani, K.; Mack, S.; Hunter, J. G.; Kates, S. L.; Daiss, J. L.; Schwarz, E. M. *J Orthop Res* **2014**, *32*, 1389−1396.
(12) Kates, S. L.; Owen, J. R.; Beck, C. A.; Xie, C.; Muthukrishnan, G.; Daiss, J. L.; Schwarz, E. M. *J Bone Joint Surg Am* **2020**, *102*, 1842−1848.
(13) Lee, C. C.; Southgate, R. D.; Jiao, C.; Gersz, E.; Owen, J. R.; Kates, S. L.; Beck, C. A.; Xie, C.; Daiss, J. L.; Post, V.; Moriarty, T. F.; Zeiter, S.; Schwarz, E. M.; Muthukrishnan, G. *Eur Cell Mater* **2020**, *39*, 96−107.
(14) Mace, C. R.; Yadav, A. R.; Miller, B. L. *Langmuir* **2008**, *24*, 12754−12757.
(15) Yadav, A. R.; Mace, C. R.; Miller, B. L. *Anal. Chem.* **2014**, *86*, 1067−1075.
(16) Bucukovski, J.; Carter, J. A.; Striemer, C. C.; Mullner, S.; Schulte-Pelkum, J.; Schulz-Knappe, P.; Miller, B. L. *J. Immunol. Methods* **2018**, *459*, 44−49.
(17) Bucukovski, J.; Latorre-Margalef, N.; Stallknecht, D. E.; Miller, B. L. *PLoS One* **2015**, *10*, No. e0134484.
(18) Tholen, D.; Linnet, K.; Kondratovich, M.; Armbruster, D.; Garrett, P. E.; Jones, R.; Kroll, M.; Lequin, R. M.; Pankratz, T.; Scassellati, G.; Schimmel, H.; Tsai, J. In *Protocols for Determination of Limits of Detection and Limits of Quantitation; Approved Guidelines*, 2004.
(19) Holstein, C. A.; Griffin, M.; Hong, J.; Sampson, P. D. *Anal. Chem.* **2015**, *87*, 9795−9801.
(20) Klose, A. M.; Miller, B. L. *Sensors (Basel)* **2020**, *20*, 5745.
(21) McKinney, W. M., & others., Data Structures for Statistical Computing in Python. *Proceedings of the 9th Python in Science Conference* 2010, *445*, 51−56.
(22) Waskom, M. L. *J. Open Source Softw.* **2021**, *6*, 3021.
(23) Jarmoskaite, I.; AlSadhan, I.; Vaidyanathan, P. P.; Herschlag, D. *Elife* **2020**, *9*, No. e57264.
(24) Meyer, T. C.; Michalik, S.; Holtfreter, S.; Weiss, S.; Friedrich, N.; Volzke, H.; Kocher, T.; Kohler, C.; Schmidt, F.; Broker, B. M.; Volker, U. *Front Immunol* **2021**, *12*, 651619.
(25) Zhang, H.; Henry, C.; Anderson, C. S.; Nogales, A.; DeDiego, M. L.; Bucukovski, J.; Martinez-Sobrido, L.; Wilson, P. C.; Topham, D. J.; Miller, B. L. *Anal. Chem.* **2018**, *90*, 9583−9590.
(26) Steiner, D. J.; Cognetti, J. S.; Luta, E. P.; Klose, A. M.; Bucukovski, J.; Bryan, M. R.; Schmuke, J. J.; Nguyen-Contant, P.; Sangster, M. Y.; Topham, D. J.; Miller, B. L. *Biosens. Bioelectron.* **2020**, *169*, 112643.
(27) Haddad, N. S.; Nozick, S.; Kim, G.; Ohanian, S.; Kraft, C.; Rebolledo, P. A.; Wang, Y.; Wu, H.; Bressler, A.; Le, S. N. T.; Kuruvilla, M.; Cannon, L. E.; Lee, F. E.; Daiss, J. L. *J. Immunol. Methods* **2021**, *492*, 112932.
(28) Haddad, N. S.; Nguyen, D. C.; Kuruvilla, M. E.; Morrison-Porter, A.; Anam, F.; Cashman, K. S.; Ramonell, R. P.; Kyu, S.; Saini, A. S.; Cabrera-Mora, M.; Derrico, A.; Alter, D.; Roback, J. D.; Horwath, M.; O'Keefe, J. B.; Wu, H. M.; Wong, A. I.; Dretler, A. W.; Gripaldo, R.; Lane, A. N.; Wu, H.; Chu, H. Y.; Lee, S.; Hernandez, M.; Engineer, V.; Varghese, J.; Patel, R.; Jalal, A.; French, V.; Guysenov, I.; Lane, C. E.; Mengistsu, T.; Normile, K. E.; Mnzava, O.; Le, S.; Sanz, I.; Daiss, J. L.; Lee, F. E. *Immunohorizons* **2021**, *5*, 322−335.
(29) Halliley, J. L.; Kyu, S.; Kobie, J. J.; Walsh, E. E.; Falsey, A. R.; Randall, T. D.; Treanor, J.; Feng, C.; Sanz, I.; Lee, F. E. *Vaccine* **2010**, *28*, 3582−3587.
(30) Lee, F. E.-H.; Falsey, A. R.; Halliley, J. L.; Sanz, I.; Walsh, E. E. *J Infect Dis* **2010**, *202*, 1659−1666.
(31) Lee, F. E.-H.; Halliley, J. L.; Walsh, E. E.; Moscatiello, A. P.; Kmush, B. L.; Falsey, A. R.; Randall, T. D.; Kaminiski, D. A.; Miller, R. K.; Sanz, I. *J. Immunol.* **2011**, *186*, 5514−5521.
(32) Raqib, R.; Mondal, D.; Karim, M. A.; Chowdhury, F.; Ahmed, S.; Luby, S.; Cravioto, A.; Andersson, J.; Sack, D. *Clin. Vaccine Immunol.* **2009**, *16*, 521−527.

https://doi.org/10.1021/acs.analchem.1c02658
Anal. Chem. 2021, 93, 13580−13588